

Original paper

Miscibility between synthetic FeS and TiS: An insight into the phase relations in natural Ti-bearing iron monosulfides

Noemi MÉSZÁROSOVÁ^{1,2*}, Roman SKÁLA^{1,2}, Petr MIKYSEK¹, Milan DRÁBEK^{3†}¹ Institute of Geology of the Czech Academy of Sciences, Rozvojová 269, 165 00 Prague 6; meszarosova@gli.cas.cz² Institute of Geochemistry, Mineralogy and Mineral Resources, Faculty of Science, Charles University in Prague, Albertov 6, 128 43 Prague 2, Czech Republic³ Czech Geological Survey, Klárov 3, 118 21 Prague 1, Czech Republic

* Corresponding author

† deceased on December 9, 2020



Syntheses of (Fe,Ti)S analogs of natural Ti-bearing troilites were performed in evacuated and sealed silica glass tubes to investigate the extent of the knowledge on the solid solution between FeS and TiS. The synthesized (Fe,Ti)S phases were investigated using electron probe microanalysis and powder X-ray diffraction. The synthetic phases of the (Fe,Ti)S series adopt NiAs-type structure of $P6_3/mmc$ space group in the compositional range from FeS to $Fe_{0.5}Ti_{0.5}S$. Members of the series rich in titanium crystallize in the $R\bar{3}m$ space group. The stoichiometric TiS can adopt both structure types. Some additional diffraction peaks were observed in numerous samples. However, due to the insufficient quality of powder XRD data, crystal structure parameters of only samples with troilite 2C superstructure could be successfully refined. Systematic variation of deficit in metal ($Me = Fe+Ti$) site occupancy with titanium content was observed in the synthetic samples. This deficit increases with the increasing Ti content in a compositional range from pure FeS to $Fe_{0.2}Ti_{0.8}S$. In samples containing more titanium than this composition, the deficit of the metal site occupancy decreases, and the composition of end-member TiS is very close to the ideal stoichiometry.

Keywords: Ti-bearing iron monosulfide, FeS–TiS solid solution, enstatite-rich meteorites, aubrites, reducing conditions

Received: 4 July 2021; **accepted:** 1 December 2021; **handling editor:** F. Laufek

1. Introduction

The group of iron monosulfides commonly occurring in nature includes troilite, pyrrhotite, and smythite. Their structures are based on the hexagonal nickel arsenide structure (NiAs-type). Structures relevant to this study are shown and described in Fig. 1. The most common of them is pyrrhotite which belongs among the most common iron sulfides in the Earth's crust. It also occurs in meteorites, especially in carbonaceous chondrites. Pyrrhotite is a non-stoichiometric mineral and its composition is expressed by the empirical formula $Fe_{1-x}S$, where $x \leq 0.125$. A large number of superstructures result from the ordering of the Fe-filled sites and vacancies. Troilite is a stoichiometric iron monosulfide mostly known from meteorites. However, some of the terrestrial occurrences have been reported in highly reducing environments (Langenhorst et al. 2013; Rubin and Ma 2017). Troilite crystallizes in the space group $P\bar{6}2c$ a superstructure of NiAs-type structure (Evans 1970; Töpel-Schadt and Müller 1982; Skála et al. 2006; Makovicky 2006). The structure of $P\bar{6}2c$ is stable at ambient conditions, and above temperatures higher than 210 °C, the structure changes into NiAs-type structure of $P6_3/mmc$ space group. Smythite is a rare mineral with even more deficit

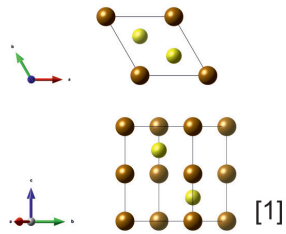
in iron than pyrrhotite with ideal composition $Fe_{13}S_{16}$, although most closely are represented by the formula Fe_9S_{11} (Fleet 1982; Langenhorst et al. 2013). It crystallizes in $R\bar{3}m$ rhombohedral space group.

Substitution of variable amounts of titanium in the structure of iron monosulfides is well known from enstatite-rich meteorites. Enstatite-rich meteorites include enstatite chondrites, which are divided based on their bulk composition into two groups: EH (high bulk iron) and EL (low bulk iron), enstatite achondrites (aubrites), and some anomalous unclassified meteorites (Keil 1968, 1969, 1989; 2010; Weyrauch et al. 2018 and references therein). Enstatite-rich meteorites formed under highly reducing conditions which are also reflected in their mineralogy. Mineralogical composition mainly consists of nearly Fe-free enstatite, Si-bearing Fe-Ni metal, and sulfides. Among them, troilite is the most abundant. Due to highly reducing conditions, some otherwise lithophile elements behaved as chalcophile and formed sulfides e.g., oldhamite (CaS), niningerite (MgS), daubréelite ($FeCr_2S_4$), heideite $(Fe,Cr)_{1+x}(Ti,Fe)_2S_4$ where $x \leq 0.15$. The reducing conditions also affected the composition of troilites as they bear lower or higher amounts of chromium and titanium. The amounts of Ti concentration in troilite vary greatly between enstatite chondrites and

NiAs-type structure and its superstructures

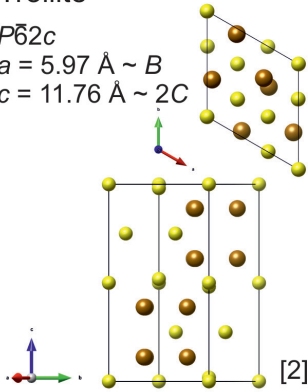
NiAs-type structure

$P6_3/mmc$
 $a \sim 3.6 \text{ \AA} = A$
 $c \sim 5 \text{ \AA} = C$
 Wyckoff positions: 2a, 2b



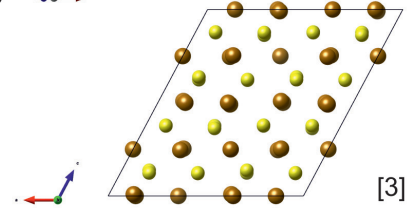
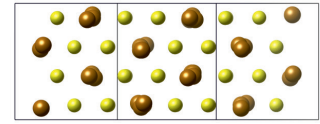
Troilite

$P\bar{6}2c$
 $a = 5.97 \text{ \AA} \sim B$
 $c = 11.76 \text{ \AA} \sim 2C$



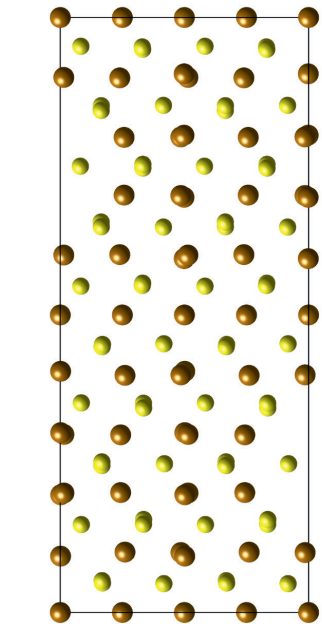
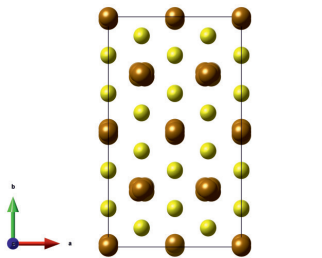
Pyrrhotite-4C

$C2/c$
 $a = 11.93 \text{ \AA}$
 $b = 6.88 \text{ \AA}$
 $c = 12.92 \text{ \AA}$
 $\alpha = 90^\circ$
 $\beta = 118^\circ$
 $\gamma = 90^\circ$



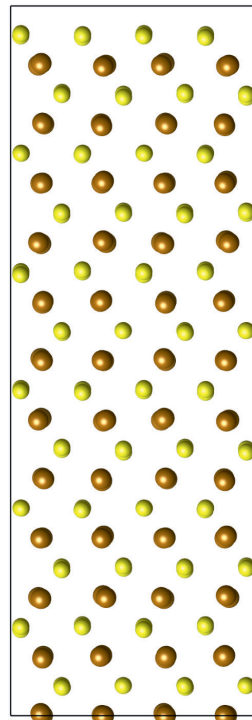
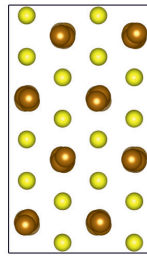
Pyrrhotite-5C

$Cmca$
 $a = 6.89 \text{ \AA} \sim 2A$
 $c = 28.63 \text{ \AA} \sim 5C$



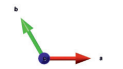
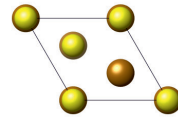
Pyrrhotite-6C

Cc
 $a = 6.90 \text{ \AA}$
 $b = 11.95 \text{ \AA}$
 $c = 28.63 \text{ \AA}$
 $\alpha = 90^\circ$
 $\beta = 101^\circ$
 $\gamma = 90^\circ$



Wassonite-type

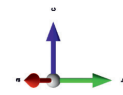
$R\bar{3}m$
 $a = 3.42 \text{ \AA}$
 $c = 26.46 \text{ \AA}$



[4]



[5]



[6]

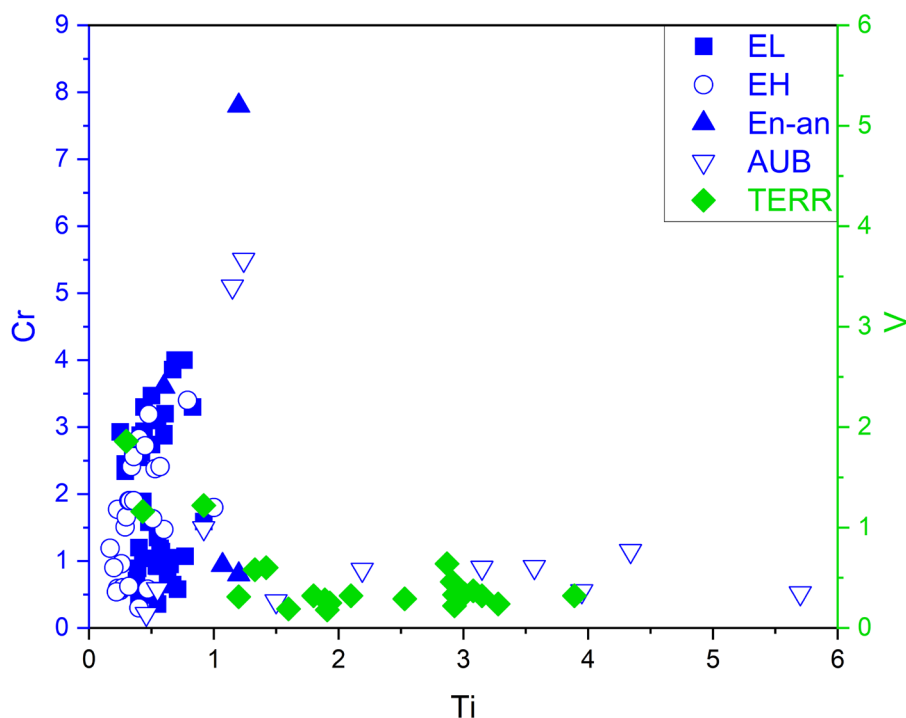
[1] Alsen (1925); [2] Skála et al. 2006; [3] Powell et al. (2004); [4] de Villiers et al. (2009); [5] de Villiers and Liles (2010); [6] Hahn and Harder (1957)

Fig. 2 Variation of titanium content is shown as dependences of the concentrations of titanium and chromium for troilites from enstatite-rich meteorites. Commonly used abbreviations for different types of enstatite-rich meteorites were adopted to identify the data. Variation of titanium content is shown as dependences of the concentrations of titanium and vanadium for Ti-bearing pyrrhotites and is marked with the abbreviation TERR.

Analytical data were taken from Barkov et al (1997, 2000) and Yakovleva et al. (2010) for terrestrial samples. Those for enstatite-rich meteorites were taken from Keil (1968, 2010), Buseck and Holsworth (1972), Olsen et al. (1977), Watters and Prinz (1979), Rambaldi et al. (1983), Nagahara and El Goresy (1984), Nehru et al. (1984), Zhang et al. (1995), Fogel (1997), Weisberg et al. (1997), Lin and Kimura (1998), Hochleitner et al. (2004), Kimura et al. (2005), Rubin and Wasson (2011), Horstmann (2013), Weyrauch et al. (2018).

aubrites (Fig. 2). A rare Ti-bearing iron monosulfide (pyrrhotite) is reported from the Khibina alkaline complex in Russia (Barkov et al. 1997, 2000; Yakovleva et al. 2010). Conditions of origin of the mineral assemblages containing the Ti-bearing pyrrhotite had to be highly reducing as they consist of Ti-bearing pyrite and marcasite, troilite, alabandite, edgarite, and others. In contrast with Ti-bearing troilites from enstatite-rich meteorites, the Ti-bearing pyrrhotite does not contain any chromium; it contains variable amounts of vanadium. Moreover, troilites coexisting with Ti-bearing pyrrhotite at that locality do not contain any titanium, chromium, or vanadium.

Stoichiometric TiS has been known only from experimental studies for a long time (Vieane and Kullerud 1971; Mitsui et al. 2009 and references therein). However, then it was discovered in the barred olivine (BO) chondrule of Yamato 691 (EH3) chondrite and named wassonite (Nakamura-Messenger et al. 2012). Due to the submicroscopic size of the studied grains, both chemical and structural characterization was performed only by transmission electron microscopy (TEM) techniques. Chemical characterization of wassonite revealed a minor amount of chromium and iron substitutions, and therefore the empirical formula corresponds to $(\text{Ti}_{0.93}\text{Fe}_{0.06}\text{Cr}_{0.01})\text{S}$. Collected selected-area electron diffraction patterns are compatible with $R\bar{3}m$ space group, also corroborated by the experimental work on Fe–Ti–S system (Vieane and



Kullerud 1971; Mitsui et al. 2009 and references therein). Experimental studies also showed that TiS might possess the structure $P6_3/mmc$, the same as for high-temperature modification of troilite and pyrrhotite (Töpel-Schadt and Müller 1982; Mitsui et al. 2009). Mitsui et al. (2009) revealed the existence of a homogenous solid solution of NiAs-type structure at temperatures 726.85 °C and higher in the study of the FeS–TiS system.

The aim of this study is a reexamination of the crystal structures of synthetic phases of the FeS–TiS system and a comparison of results with the naturally occurring Ti-bearing iron monosulfides, especially the Ti-bearing troilites known from enstatite-rich meteorites.

2. Samples and experimental methods

The polished thin section M5635 of Bustee meteorite (aubrite) from the meteorite collection of the Naturhistorisches Museum Wien (NHM) was used in this study to represent the natural Ti-bearing troilites from enstatite-rich meteorites.

Synthetic samples were prepared from elements of high purity, which were weighted to represent desired stoichiometry, in evacuated and sealed silica glass tubes in horizontal tube furnaces at 800 °C. The heat treatment took a different amount of time depending on the composition of the particular sample (up to 6 months for titanium-rich samples), and it ended by quenching. Polished (thin) sections were prepared from synthetic

⇐

Fig. 1 Summary of published superstructures of NiAs-type structure related to the study.

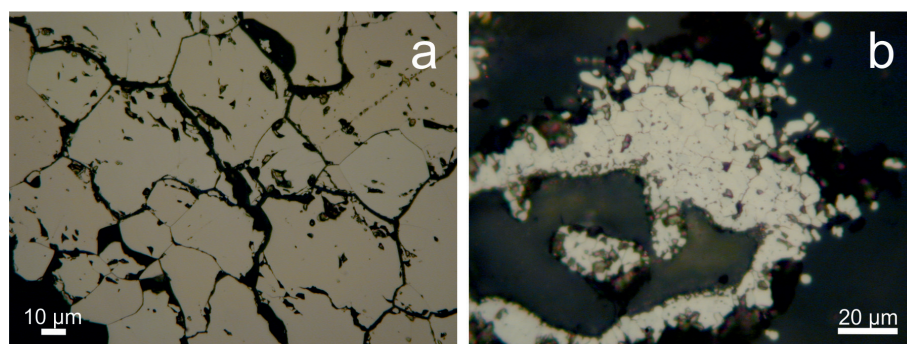


Fig. 3 The appearance of the synthetic samples in the polished sections in reflected light. **a** – synthetic sample of ideal stoichiometry FeS. **b** – synthetic sample of ideal stoichiometry TiS.

samples to define their chemical composition using an electron probe microanalyzer (EPMA).

The chemical composition of the synthetic samples and Ti-bearing troilite grains from Bustee was measured with a JEOL JXA-8200 SuperProbe electron probe microanalyzer (BGI, Bayreuth). The accelerating voltage of 20 kV, the probe current of 20 nA, and an electron beam of 2 μm in diameter were used for the measurements. The analyzed elements included (used the spectral line, standard, and detection limit in ppm, respectively, are given in parentheses): Fe (K_{α} , FeS₂, 1500), Ti (K_{α} , MnTiO₃, 300), S (K_{α} , FeS₂, 750), and Cr (K_{α} , metal Cr, 430).

Philips X'Pert MPD diffractometer in reflecting Bragg-Brentano geometry equipped with a proportional detector and graphite diffracted beam monochromator was used to collect diffraction data (Czech Acad. Sci., Inst. Geol., Prague). The analyses were performed under the following conditions: CuK α radiation, step size of 0.02°, counting time 3 s at each step and the 2 θ range of 10–130°. Samples were placed on zero-background silicon sample holders. Qualitative analysis was performed with ZDS-WX Search/Match X-ray diffraction software

(Ondruš and Skála 1997) teamed with the JCPDS PDF-2 database.

The Rietveld crystal structure refinements of measured samples were performed with the TOPAS V4.2 program (Bruker AXS 2008) with an initial structure model taken from Alsen (1925). Refined parameters included scale factor, coefficients of Chebyshev polynomial used to model a background, sample displacement, isotropic displacement factors, U , V , W , and X parameters of the Thompson-Cox-Hastings pseudo-Voigt profile shape function (*PSF*) (Thompson et al. 1987). When the *PSF* did not describe peak shapes satisfactorily, additional functions (Lorentzian and/or hat) were convoluted on the profile. Preferred orientation effects were treated by spherical harmonics of the 4th order. The site occupations were taken from chemical analyses and their refinement has not been attempted.

3. Results

A set of synthetic materials with different compositions along the FeS–TiS join were synthesized. Synthetic samples showed a typical bronze-yellow to pinch-beck-brown color visible in the polished sections (Fig. 3). Though, in general, the synthesized materials were fairly homogenous, the presence of unreacted iron has been shown in BSE images of samples of Fe_{0.7}Ti_{0.3}S, Fe_{0.6}Ti_{0.4}S and Fe_{0.5}Ti_{0.5}S compositions (Fig. 4). It was also noticed in powder XRD data. The amount of iron

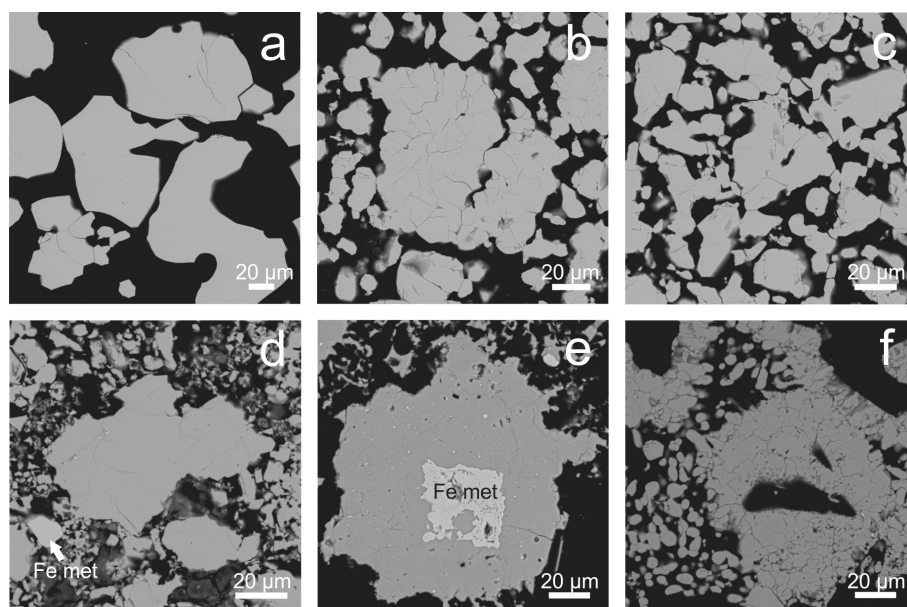


Fig. 4 BSE images of the selected synthetic samples, to describe them, the ideal stoichiometric formula is stated. **a** – FeS; **b** – Fe_{0.95}Ti_{0.05}S; **c** – Fe_{0.8}Ti_{0.2}S; **d** – Fe_{0.7}Ti_{0.3}S; **e** – Fe_{0.5}Ti_{0.5}S; **f** – TiS. Unreacted iron, if present, is labeled with the abbreviation Fe met.

Tab. 1 Unit-cell parameters of synthetic samples along FeS-TiS join quoted for NiAs-types structure. Isotropic displacement factors and common refinement agreement factors for the Rietveld analysis are reported. Abbreviation *Me* stands for a metal site in NiAs-type structure which in the case of synthetic materials consist of iron and titanium (Fe+Ti).

TiS [mol. %]	<i>a</i> [Å]	<i>c</i> [Å]	<i>V</i> [Å ³]	<i>c/a</i>	<i>B_{eq}Me</i> [Å ²]	<i>B_{eq}S</i> [Å ²]	<i>R_{Bragg}</i> [%]	<i>R_{exp}</i> [%]	<i>R_{wp}</i> [%]	<i>R_p</i> [%]	<i>GOF</i>
0	3.4454(2)	5.8783(3)	60.432(6)	1.7062(3)	3.20(9)	0.95(9)	4.088	16.87	19.67	14.25	1.17
5	3.4474(1)	5.8234(2)	59.937(5)	1.6892(2)	1.83(7)	0.77(7)	4.514	17.94	22.46	15.81	1.25
10	3.4486(1)	5.8214(3)	59.959(5)	1.6880(2)	2.48(8)	0.89(7)	4.058	18.53	22.42	16.68	1.21
20	3.4481(1)	5.8128(2)	59.850(3)	1.6858(1)	2.5(1)	0.80(1)	2.935	17.29	19.56	14.40	1.13
30	3.4487(1)	5.8003(2)	59.744(4)	1.6819(2)	2.79(9)	0.68(8)	3.151	17.26	20.25	15.17	1.17
40	3.4422(1)	5.7976(2)	59.492(3)	1.6843(1)	2.17(6)	0.21(5)	4.103	14.92	17.67	13.24	1.18
50	3.4297(1)	5.8112(3)	59.199(5)	1.6944(2)	2.1(1)	0.40(3)	3.172	19.23	20.77	15.81	1.08
100	3.3100(1)	6.3482(3)	60.235(6)	1.9179(2)	0.68(5)	0.33(5)	2.620	15.28	18.63	12.90	1.22

was refined during the Rietveld crystal structure refinement and it was around 3 wt. % and the maximum value was 6 wt. % in the sample with the empirical formula $\text{Fe}_{0.5}\text{Ti}_{0.5}\text{S}$.

Generally, iron-rich members of the series crystallize in the NiAs-type structure of the $P6_3/mmc$ space group. The NiAs-type structure is observed in a compositional region between pure FeS and $\text{Fe}_{0.5}\text{Ti}_{0.5}\text{S}$ and is also met in phases chemically close to pure TiS. The powder X-ray diffraction (XRD) pattern of the experimental charge with the composition of $\text{Fe}_{0.4}\text{Ti}_{0.6}\text{S}$ showed a mixture of the NiAs-type-structured (dominant) and the wassonite-type-structured ($R\bar{3}m$) phases. Members of the series rich in titanium were found to crystallize in the wassonite-type structure. The wassonite-type structure was also observed in one case of the pure TiS member. Results of refinement of unit-cell parameters for experiments refined with NiAs-type structures are listed in Tab. 1. and representative Rietveld refinement plots are plotted in Fig. 5.

Some additional diffraction peaks of variable intensity were observed in several synthetic samples. We believe that those diffraction peaks could correspond to superstructures of NiAs-type. Attempts of refinement of superstructures were

made using superstructures known from the literature. However, it was successful only in the case of troilite (2C pyrrhotite) superstructures due to the insufficient quality of the powder XRD data of the synthetic samples. The initial structure model was taken from Skála et al. (2006).

Nevertheless, during the refinement, at least two additional superstructures have been recognized. In the case of synthetic samples with only a small amount of titanium, the superstructure appears to correspond to pyrrhotite 3C. The initial structure model was taken from Nakano et al. (1979). In the compositional range around the middle of the solid solution, the superstructure seems to be consistent with the pyrrhotite 5C superstructure. The initial structure model was taken from de Villiers et al. (2009).

The chemical composition of the synthetic samples is summarized in Tab. 2. The empirical formulas were

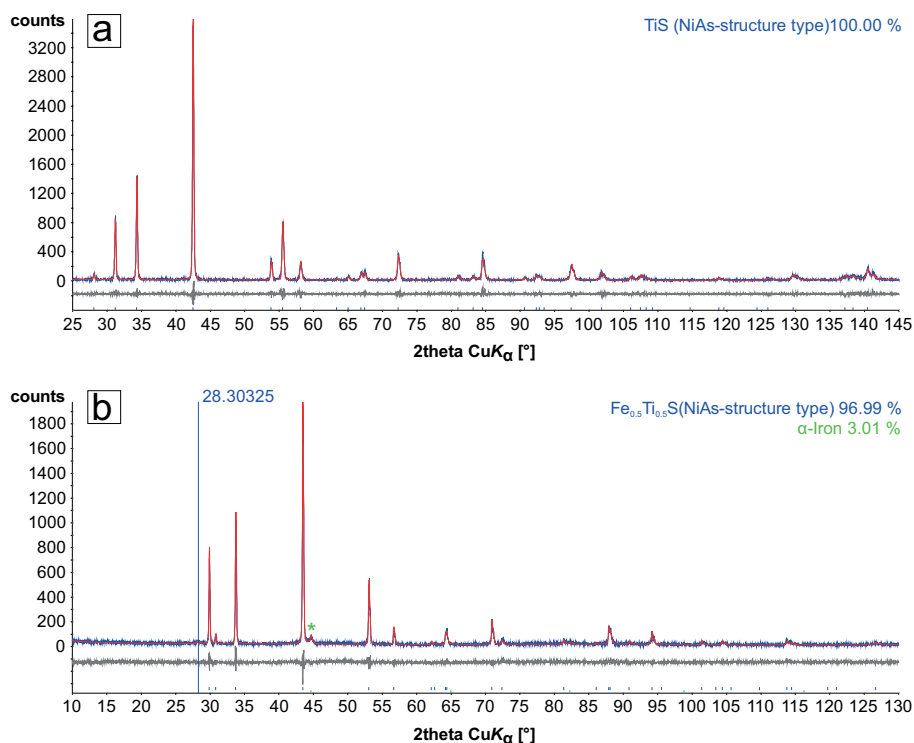


Fig. 5 Representative Rietveld refinement plots of **a** – synthetic stoichiometric TiS; **b** – synthetic stoichiometric $\text{Fe}_{0.5}\text{Ti}_{0.5}\text{S}$. A small amount of unreacted α -iron is present; a green asterisk marks its most intensive diffraction peak. The diffraction peak at $\sim 28.3^\circ$ 2θ $\text{CuK}\alpha_1$ could probably belong to one of the superstructures. For both plots, the blue curve represents powder XRD data, red is the curve calculated by the Rietveld refinement, and the difference curve is grey.

Tab. 2 Chemical composition of synthetic Ti-bearing iron monosulfides. Empirical formulas were calculated based on one atom of sulfur per formula unit.

wt. %	<i>n</i>	S	Ti	Cr	Fe	Total
FeS	20	36.62 ± 0.14	b.d.l.	b.d.l.	62.34 ± 0.32	98.96 ± 0.37
Fe _{0.991} Ti _{0.009} S	5	37.17 ± 0.39	0.44 ± 0.01	b.d.l.	61.83 ± 0.44	99.46 ± 0.47
Fe _{0.95} Ti _{0.05} S	10	37.03 ± 0.14	5.15 ± 0.03	b.d.l.	56.76 ± 0.24	98.94 ± 0.36
Fe _{0.8} Ti _{0.2} S	10	37.99 ± 0.10	11.30 ± 0.04	b.d.l.	49.84 ± 0.23	99.14 ± 0.21
Fe _{0.7} Ti _{0.3} S	10	39.40 ± 0.34	17.76 ± 0.08	b.d.l.	42.50 ± 0.34	99.66 ± 0.48
Fe _{0.6} Ti _{0.4} S	10	40.91 ± 0.31	24.95 ± 0.10	b.d.l.	33.90 ± 0.25	99.77 ± 0.32
Fe _{0.5} Ti _{0.5} S	10	42.19 ± 0.30	31.37 ± 0.17	b.d.l.	26.47 ± 0.27	100.04 ± 0.37
Fe _{0.4} Ti _{0.6} S	11	43.02 ± 0.31	37.90 ± 0.40	b.d.l.	18.92 ± 0.48	99.85 ± 0.41
Fe _{0.2} Ti _{0.8} S	10	44.06 ± 0.23	53.28 ± 0.18	b.d.l.	2.13 ± 0.34	99.48 ± 0.31
Fe _{0.1} Ti _{0.9} S	10	42.80 ± 0.16	56.77 ± 0.13	b.d.l.	0.13 ± 0.08	99.71 ± 0.17
Fe _{0.05} Ti _{0.95} S	12	41.55 ± 0.99	57.95 ± 0.99	b.d.l.	0.12 ± 0.03	99.59 ± 0.32
TiS	10	40.11 ± 0.48	59.87 ± 0.36	b.d.l.	b.d.l.	100.00 ± 0.77

apfu	<i>n</i>	Ti	Fe	<i>Me</i>	Deficit %
FeS	20	–	0.978 ± 0.006	0.978 ± 0.006	2.24
Fe _{0.991} Ti _{0.009} S	5	0.0079 ± 0.0002	0.955 ± 0.014	0.963 ± 0.014	3.71
Fe _{0.95} Ti _{0.05} S	10	0.0932 ± 0.0007	0.880 ± 0.002	0.973 ± 0.002	2.67
Fe _{0.8} Ti _{0.2} S	10	0.1993 ± 0.0007	0.753 ± 0.005	0.952 ± 0.007	4.75
Fe _{0.7} Ti _{0.3} S	10	0.3020 ± 0.0031	0.619 ± 0.007	0.921 ± 0.009	7.86
Fe _{0.6} Ti _{0.4} S	10	0.409 ± 0.004	0.476 ± 0.005	0.884 ± 0.009	11.56
Fe _{0.5} Ti _{0.5} S	10	0.498 ± 0.002	0.360 ± 0.005	0.858 ± 0.007	14.17
Fe _{0.4} Ti _{0.6} S	11	0.590 ± 0.005	0.253 ± 0.007	0.843 ± 0.005	15.74
Fe _{0.2} Ti _{0.8} S	10	0.810 ± 0.005	0.028 ± 0.004	0.838 ± 0.006	16.23
Fe _{0.1} Ti _{0.9} S	10	0.888 ± 0.004	0.002 ± 0.001	0.890 ± 0.004	10.98
Fe _{0.05} Ti _{0.95} S	12	0.935 ± 0.038	0.0005 ± 0.008	0.936 ± 0.039	6.45
TiS	10	1.000 ± 0.009	–	1.000 ± 0.009	0.02

b.d.l. – concentration below the limits of the detection.

calculated from EPMA data based on one sulfur atom in the formula unit. Variable amounts of deficit in the metal site ($Me = Fe + Ti + Cr$) were found out in these formulas

(Fig. 6). The deficit in the metal site increases with the increasing Ti content. After reaching the level of ca 80 mol. % of TiS, the degree of deficit gradually ceases until

the phases with compositions close to the end-member TiS attain almost ideal stoichiometry.

The chemical composition of Ti-bearing troilites from Bustee is listed in Tab. 3. Amounts of titanium vary greatly among the individual grains of troilite. The variable amount of the Me deficit is plotted in Fig. 6. Usually, the

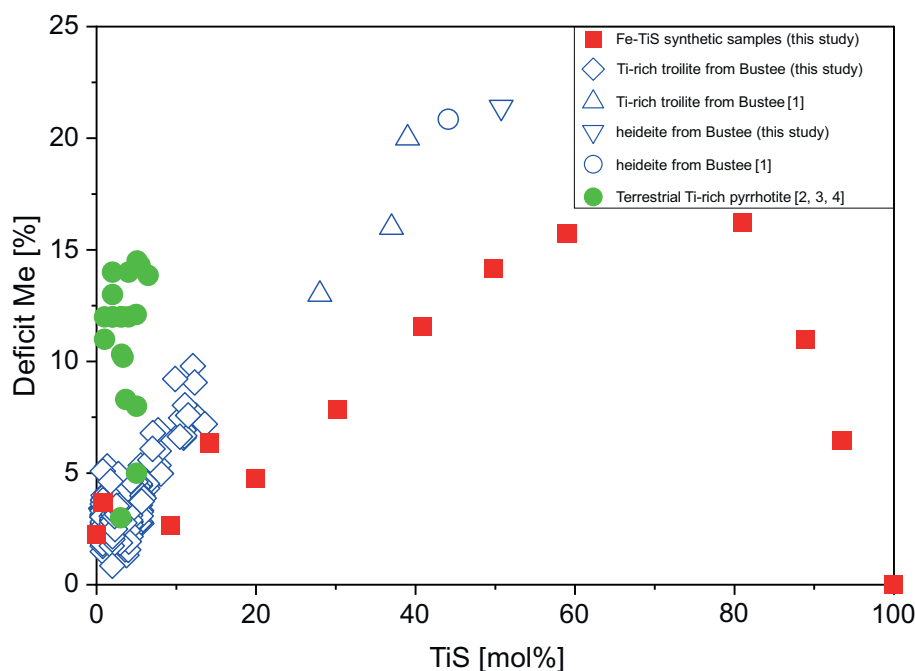


Fig. 6 Variation of the Me ($Fe + Ti$) site deficit in the NiAs-type structure on the composition of the synthesized $(Fe,Ti)S$ phases. For comparison, the composition of natural Ti-bearing troilites and heideites from Bustee aubrite and Ti-bearing pyrrhotites from the Khibina alkaline complex have been plotted. In natural samples, the contribution of other substituted elements, mostly chromium (meteoritical) and vanadium (terrestrial), is treated like iron.

[1] McCoy (1998); [2,3] Barkov et al. (1997, 2010); [4] Yakovleva et al. (2010)

Tab. 3 Chemical composition of natural Ti-bearing troilites from Bustee aubrite. Empirical formulas were calculated based on one atom of sulfur per formula unit.

wt. %	<i>n</i>	S	Ti	Cr	Fe	Total
	40	36.94 ± 0.20	0.42 ± 0.04	0.31 ± 0.11	61.47 ± 0.43	99.14 ± 0.46
analyses of troilites grouped together based on similar titanium concentration	25	36.91 ± 0.22	0.89 ± 0.10	0.31 ± 0.05	60.86 ± 0.54	98.97 ± 0.64
	33	36.97 ± 0.17	1.12 ± 0.03	0.31 ± 0.06	60.58 ± 0.23	98.98 ± 0.30
	12	36.93 ± 0.20	1.45 ± 0.09	0.49 ± 0.33	59.79 ± 0.51	98.66 ± 0.40
	16	36.97 ± 0.21	2.11 ± 0.19	0.41 ± 0.25	59.53 ± 0.54	99.03 ± 0.41
	10	37.29 ± 0.16	3.09 ± 0.22	0.43 ± 0.04	57.90 ± 0.36	98.71 ± 0.29
	8	37.62 ± 0.16	4.19 ± 0.29	0.43 ± 0.10	56.32 ± 0.36	98.84 ± 0.39
	8	37.98 ± 0.21	6.34 ± 0.24	0.60 ± 0.11	53.53 ± 0.33	98.45 ± 0.26
wt. %	No.	S	Ti	Cr	Fe	Total
individual analysis of troilite grain	376	38.41	7.50	0.67	51.55	98.13
	377	38.35	7.54	0.59	52.78	99.26
	379	38.55	7.58	0.60	52.15	98.88
	271	38.18	8.29	0.57	52.08	99.12
<i>apfu</i>	<i>n</i>	Ti	Cr	Fe	<i>Me</i>	Deficit %
analyses of troilites grouped together based on similar titanium concentration	40	0.008 ± 0.001	0.005 ± 0.002	0.956 ± 0.007	0.969 ± 0.007	3.08
	25	0.018 ± 0.002	0.005 ± 0.001	0.947 ± 0.010	0.969 ± 0.011	3.05
	33	0.022 ± 0.001	0.005 ± 0.001	0.941 ± 0.005	0.968 ± 0.005	3.19
	12	0.028 ± 0.002	0.008 ± 0.005	0.930 ± 0.010	0.966 ± 0.007	3.42
	16	0.041 ± 0.003	0.007 ± 0.004	0.925 ± 0.012	0.972 ± 0.010	2.77
	10	0.058 ± 0.004	0.007 ± 0.001	0.891 ± 0.006	0.956 ± 0.005	4.38
	8	0.075 ± 0.005	0.007 ± 0.002	0.859 ± 0.008	0.942 ± 0.007	5.84
8	0.107 ± 0.004	0.010 ± 0.002	0.809 ± 0.007	0.926 ± 0.009	7.37	
<i>apfu</i>	No.	Ti	Cr	Fe	<i>Me</i>	Deficit %
individual analysis of troilite grain	376	0.121	0.011	0.771	0.902	9.79
	377	0.124	0.010	0.790	0.924	7.57
	379	0.123	0.010	0.777	0.909	9.06
	271	0.136	0.009	0.783	0.928	7.20

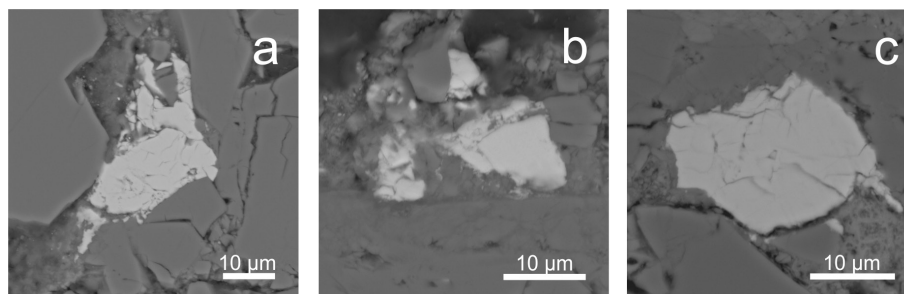
troilite grains were relatively small in size and solitary surrounded by enstatite (Fig. 7). One unique grain of heideite was found during the study in the polished (thin) section (Fig. 7). Its measured chemical composition is (in wt. %) S 44.79, Ca 0.56, Ti 33.93, Cr 5.75, Fe 14.25 and Ni 0.55 with a total 99.83; and corresponding empirical formula calculated based on 4 sulfur atoms is $(\text{Fe}_{0.731}, \text{Cr}_{0.317}, \text{Ni}_{0.027}, \text{Ca}_{0.040})_{\Sigma 1.11} \text{Ti}_{2.030} \text{S}_4$.

4. Discussion

Although a small part of the iron remained unreacted in some of the synthesized samples, unreacted sulfur has

not been found in any sample. It is not probable that this phenomenon could cause a deficit in the metal site of the samples. Although some samples contain a small amount of unreacted iron, the percentage of refined amounts of iron is much lower than the percentage of the Me deficit. The amount of iron refined from powder XRD data is 6 wt. % in sample $\text{Fe}_{0.5}\text{Ti}_{0.5}\text{S}$, which has the Me deficit of 14 % with actual empirical formula $\text{Fe}_{0.360}\text{Ti}_{0.498}\text{S}$ calculated from the EPMA analyses. Unfortunately, the results of the chemical compositions measured by EPMA have not been published for the synthetic material reported by Mitsui et al. (2009). Consequently, it is impossible to compare their results with our observation that indicates the partly vacant metal site in the synthe-

Fig. 7 BSE images of representative grains of Ti-bearing troilites (**a**, **b**) and heideite (**c**) from Bustee aubrite. **a** – Ti-bearing troilite with an average titanium concentration of ~ 3.8 wt. % is surrounded with enstatite; **b** – Grain of the most titanium enriched Ti-bearing troilite found in this study. It contains ~ 8 wt. % of Ti, and it is surrounded with enstatite; **c** – The only grain of heideite found in the study and it is surrounded with enstatite (darker in BSE) and diopside (brighter in BSE).



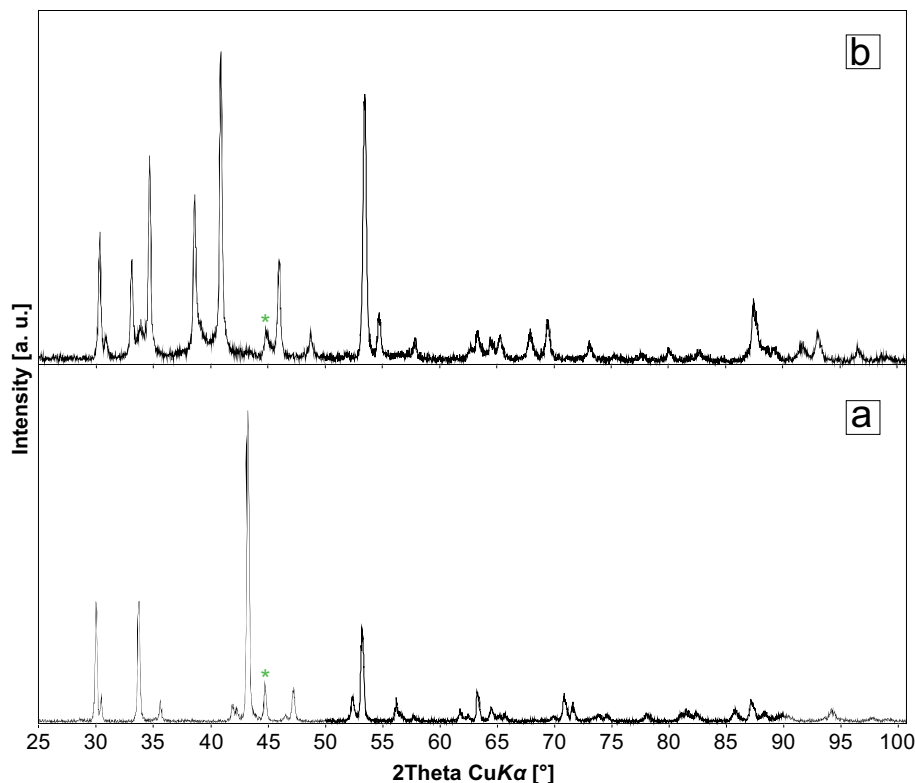


Fig. 8 Comparison of the powder X-ray patterns of the studied synthetic samples with structure **a** – $P-62c$ of pure FeS and **b** – $R-3m$ of Ti-bearing synthetic phase with composition $Fe_{0.1}Ti_{0.9}S$; * indicates the diffraction due to admixture of iron.

sized (FeTi)S phases. Nevertheless, natural Ti-bearing troilites also show a partly vacant metal site. The deficit at the metal site has been stated by McCoy (1998) and Buseck and Holdsworth (1972). Notably, Buseck and Holdsworth (1972) studied troilites from enstatite chondrite Yilmia, which contained a significantly smaller amount of titanium than troilites from Bustee studied by McCoy (1998), which are very rich in titanium.

McCoy (1998) suggested a trend in titanium enrichment in the chemical composition of Ti-bearing troilites from Bustee toward heideite and a possibility of a solid solution between troilite and heideite. For better visualization, analyses of heideite (from this study and published by McCoy 1998) were recalculated on the basis of one sulfur atom per formula unit and plotted in Fig. 6. The deficit of the metal position for natural heideite

is greater than 20 %. Heideite has a disordered NiAs-type structure crystallizing in monoclinic space group $I2/m$ (Keil and Brett 1974 and references therein). This structure contains cation layers with ordered vacancies alternating with the cation layer fully occupied. Nakajima et al. (1972) suggested for synthetic $(Fe,Ti)_3S_4$ (i.e., $(Fe,Ti)_{0.75}S$ on one sulfur per formula unit) that the fully occupied layers are filled with Ti atoms while partly vacant layers contain Fe atoms.

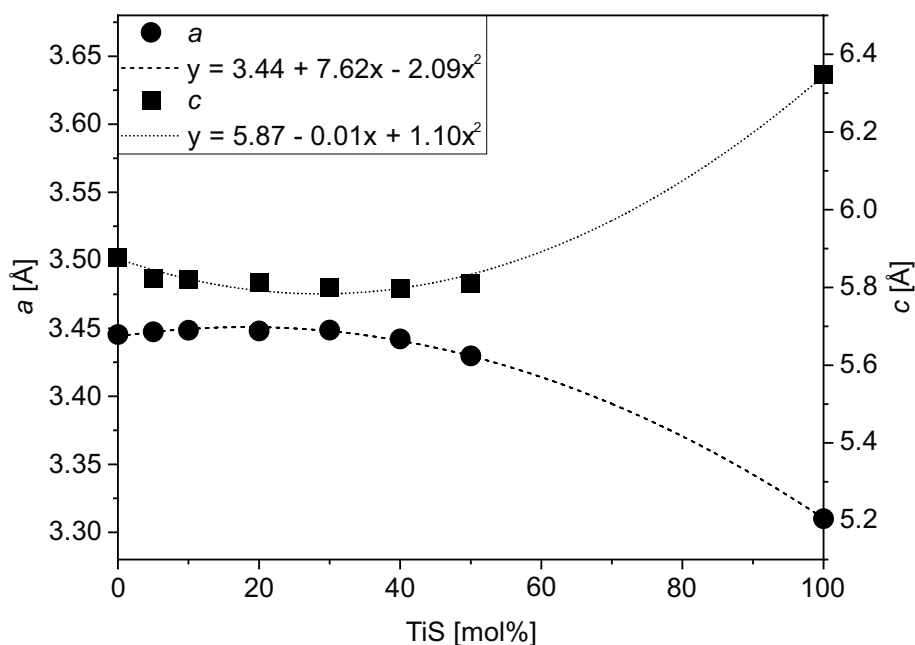


Fig. 9 Variation of the unit-cell parameters along with titanium content in studied synthetic samples. The values shown are reported for NiAs-type structure.

Similar *Me* deficits in the metal site as those observed for synthetic phases prepared in this study have been reported by Schrader et al. (2021) in pyrrhotites from carbonaceous and ordinary chondrites. Considering the chemical composition solely, the synthesized (Fe,Ti)S phases could correspond to Ti-bearing pyrrhotites considering the vacancies in the metal site. Consequently, it is questionable if the same approach could also be applicable for Ti-bearing troilites reported from Bustee aubrite (McCoy 1998).

Likewise, the synthetic samples and iron monosulfides from meteorites, the terrestrial Ti-bearing pyrrhotites showed significant variability in titanium (and vanadium) concentration and the *Me* (Fe+Ti+V) deficit (Figs. 2 and 6).

The results for synthetic phases given above correspond well with data already published earlier by Mitsui et al. (2009). In good agreement with their results, our samples synthesized at 800 °C revealed the NiAs-type structure in the phases of TiS composition and those from the compositional range from FeS to Fe_{0.5}Ti_{0.5}S. Also, several samples of high titanium content from the compositional region from (Fe_{0.2}Ti_{0.8})S to (Fe_{0.05}Ti_{0.95})S showed wassonite-type structure. To illustrate the difference between NiAs-type structure and its superstructures, powder XRD patterns of troilite (*P*-62*c*) and wassonite-type structure (*R*-3*m*) are shown in Fig. 8. The increase of *a* and a decrease of the *c* unit-cell parameter with rising TiS content is also in good agreement with published data (Fig. 9). Although the unit-cell parameter refinement had been carried out with NiAs-type archetype as a starting structure model, the polytype approach could give a more appropriate solution as suggested by Skála and Drábek (2005). Unfortunately, the unambiguous identification of the actual polytype for a given sample was not possible from the powder XRD data. The presence of more than only one polytype could also be a possible issue. As stated above, in the cases of Ti-rich members of the FeS–TiS system, the mixture of at least two structures (wassonite-type and probably NiAs-type) is present. Moreover, during the attempts to refine the structure as the superstructure, some of the diffraction peaks could not be assigned to the polytypic structures known from the literature. Unfortunately, it is not easy to compare the results with the outcome of the study by Mitsui et al. (2009) since they did not state any additional diffraction peaks related to superstructures or not.

Harries and Langenhorst (2013) observed in their TEM investigation of Fe,Ni-sulfides nanoscale assemblages in different carbonaceous chondrites, e.g., complex exsolution textures of pyrrhotite, troilite, and pentlandite; polycrystalline pyrrhotite-pentlandite-magnetite aggregates; and troilite-metal aggregates. The origin of a particular assemblage is controlled by the condition of formation

and/or metamorphism. They also pointed out that the small amounts of nickel measured by EPMA (around 2 wt. %) in the Y-791198 and Y-793321 meteorites are actually formed by nanosized blebs pentlandite in troilite-pyrrhotite intergrowths. Similar nanoscale assemblages could cause small amounts of titanium measured by EPMA in Ti-bearing troilites and in their synthetic analogs. Obviously, TEM investigation is needed to confirm these assumptions.

5. Conclusions

A detailed investigation of solid solution between synthetic FeS and TiS was conducted using electron probe microanalysis (EPMA) and powder X-ray diffraction. A study of the chemical composition revealed the variable deficit in the metal (*Me* = Fe+Ti) site occupation whose degree depends on the overall titanium content in the phase under scrutiny. A similar deficit of the metal site can be observed in Ti-bearing troilites in aubrites. Most of the synthetic samples of the (Fe,Ti)S series adopt the NiAs-type structure of the *P*6₃/*m**mc* space group. Synthetic samples with high titanium content adopt the wassonite-type structure of the *R*-3*m* space group. Stoichiometric TiS can adopt both structure types. Due to the deficit in the metal site occupancy and an affinity of the structures of the synthesized samples to adopt the NiAs-type superstructures, the question about assigning the synthetic samples instead to Ti-bearing pyrrhotite should be asked. Similarly, the question about the true nature of the Ti-bearing troilites from enstatite-rich meteorites will require further investigation.

Acknowledgments. This study was supported by the Institutional Research Plan RVO 67985831 of the Institute of Geology of the Czech Academy of Sciences, Prague and conducted within the support of Charles University Grant Agency, project No. 1090119. We would like to gratefully thank Franz Brandstätter for providing the sample of Bustee meteorite for this study. Furthermore, we thank Sergey Britvin for the constructive review and editor František Laufek for comments and managing the manuscript.

References

- ALSEN N (1925) Röntgenographische Untersuchungen der Kristallstrukturen von Magnetkies, Breithauptit, Pentlandit, Millerit und verwandten Verbindungen. Geol fören Stockholm förh 47:19–73
- BARKOV AY, LAAJOKI KVO, MEN'SHIKOV YP, ALAPIETI TT, SIVONEN AJ (1997) First terrestrial occurrence of

- titanium-rich pyrrhotite, marcasite and pyrite in fenitized xenolith from the Khibina alkaline complex, Russia. *Canad Mineral* 35: 875–885
- BARKOV AY, MARTIN RF, MEN'SHIKOV YP, SAVCHENKO YE, THIBAUT Y, LAAJOKI KVO (2010) Edgarite, FeNb_3S_6 , first natural niobium-rich sulfide from the Khibina alkaline complex, Russian far north: evidence for chalcophile behavior of Nb in a fenite. *Contrib Mineral Petrol* 138: 229–236
- BRUKER AXS (2008) TOPAS V4: General profile and structure analysis software for powder diffraction data. User's Manual, Bruker AXS, Karlsruhe, Germany
- BUSECK PR, HOLDSWORTH EF (1972) Mineralogy and petrology of the Yilmia enstatite chondrite. *Meteoritics* 7: 429–447
- DE VILLIERS JPR, LILES DC AND BECKER M (2009) The crystal structure of naturally occurring 5C pyrrhotite from Sudbury, its chemistry, and vacancy distribution. *Amer Miner* 94: 1405–1410
- DE VILLIERS JPR AND LILES DC (2010) The crystal-structure and vacancy distribution in 6C pyrrhotite. *Amer Miner* 95: 148–152
- EVANS HT (1970) Lunar troilite: Crystallography. *Science* 167: 73–92
- FLEET ME (1982) Synthetic smythite and monoclinic Fe_3S_4 . *Phys Chem Miner* 8: 241–246
- FOGEL RA (1997) On the significance of diopside and oldhamite in enstatite chondrites and aubrites. *Meteorit Planet Sci* 32: 577–591
- HAHN H, HARDER B (1957) Zur Kristallstruktur der Titan-sulfide. *Z Anorg Allg Chem* 288: 241–256
- HARRIES D, LANGENHORST F (2013) The nanoscale mineralogy of Fe,Ni sulfides in pristine and metamorphosed CM and CM/CI-like chondrites: Tapping a petrologic record. *Meteorit Planet Sci* 48: 879–903
- HOCHLEITNER R, FEHR KT, SIMON G, POHL J, SCHMIDBAUER E (2004) Mineralogy of ^{57}Fe Mössbauer spectroscopy of opaque phases in the Neuschwanstein EL6 chondrite. *Meteorit Planet Sci* 39: 1643–1648
- HORSTMANN M (2013) The Almahata Sitta meteorites: Insights into the nature of selected chondritic and achondritic lithologies and possible genetic relations. PhD thesis, Westfälische Wilhelms-Universität Münster, Münster, Germany
- KEIL K (1968) Mineralogical and chemical relationships among enstatite chondrites. *J Geophys Res* 73: 6945–6976
- KEIL K (1969) Titanium distribution in enstatite chondrites and achondrites, and its bearing to their origin. *Earth Planet Sci Lett* 7: 243–248
- KEIL K (1989) Enstatite meteorites and their parent bodies. *Meteoritics* 24: 195–208
- KEIL K (2010) Enstatite achondrite meteorites (aubrites) and the histories of their asteroidal parent bodies. *Chem Erde* 70: 295–317
- KEIL K, BRETT R (1974) Heideite, $(\text{Fe,Cr})_{1+x}(\text{Ti,Fe})_2\text{S}_4$, a new mineral in the Bustee enstatite achondrite. *Amer Miner* 59: 465–470
- KIMURA M, WEISBERG MK, LIN Y, SUZUKI A, OHTANI E, OKAZAKI R (2005) Thermal history of the enstatite chondrites from silica polymorphs. *Meteorit Planet Sci* 40: 855–868
- LANGENHORST F, HARRIES D, POLLOK K (2013) Non-stoichiometry, defects and superstructures in sulfide and oxide minerals. In: NIETO F, LIVI KJT (eds) *Minerals at nanoscale*. EMU Notes in Mineralogy 14, London, pp 261–295
- LIN Y, KIMURA M (1998) Petrographic and mineralogical study of new EH melt rock and a new enstatite chondrite grouplet. *Meteorit Planet Sci* 33: 501–511
- MAKOVICKY E (2006) Crystal structure of sulfides and other chalcogenides. In: VAUGHAN DJ (ed) *Sulfide mineralogy and geochemistry*. *Rev Mineral Geochem* 61, Washington DC, pp 7–125
- MCCOY TJ (1998) A pyroxene-oldhamite clast in Bustee: Igneous aubritic oldhamite and mechanism for Ti enrichment in aubritic troilite. *Antarct Meteorite Res* 11: 32–48
- MITSUI H, SASAKI T, OIKAWA K, ISHIDA K (2009) Phase equilibria in FeS–XS and MnS–XS (X=Ti, Nb and V) systems. *J Iron Steel Inst Jpn* 49: 936–941
- NAGAHARA H, EL GORESY A (1984) Yamato-74370: A new enstatite chondrite (EH4) (abstr.) 15th Lunar and Planetary Science Conference pp 583
- NAKAJIMA S, HORIUCHI H, MORIMOTO N (1972) Crystal structures of $(\text{Fe,Ti})_3\text{S}_4$ (abstr.). *Acta Crystallogr A* 28: pp 61
- NAKAMURA-MESSENGER K, CLEMETT SJ, RUBIN AE, CHOI B-G, ZHANG S, RAHMAN Z, OIKAWA K, KELLER LP (2012) Wassonite: A new titanium monosulfide mineral in the Yamato 691 enstatite chondrite. *Amer Miner* 97: 807–812
- NAKANO A, TOKONAMI M, MORIMOTO N (1979) Refinement of 3C Pyrrhotite, Fe_7S_8 . *Acta Crystallogr B* 35: 722–724
- NEHRU CE, PRINZ M, WEISBERG MK, DELANEY JS (1984) Parsa: An unequilibrated enstatite chondrite (uec) with an aubrite-like impact melt clast (abstr.) 15th Lunar and Planetary Science Conference pp 597
- OLSEN EJ, BUNCH TE, JAROSEWICH E, NOONAN AF, HUSS GI (1977) Happy Canyon: a new type of enstatite achondrite. *Meteoritics* 12: 109–123
- ONDROŠ P, SKÁLA R (1997) New quasi-empirical channel Search/Match algorithm for ICDD PDF2 Database: A tool for qualitative X-ray powder diffraction analysis. EPDIC-5, Parma: pp 193
- POWELL AV, VAQUEIRO P, KNIGHT KS, CHAPON C, SÁNCHEZ RD (2004) Structure and magnetism in synthetic pyrrhotite Fe_7S_8 : A powder neutron-diffraction study. *Phys Rev B* 70: 014415-12
- RAMBALDI ER, HOUSLEY RM, RAJAN RS, CIRLIN E, EL GORESY A, WANG D (1983) Unusual mineral assemblages

- and textures in Qingzhen enstatite chondrites. *Meteoritics* 18: 380–381
- RUBIN AE, MA C (2017) Meteoritic minerals and their origins. *Chem Erde* 77: 325–385
- RUBIN AE, WASSON JT (2011) Shock effects in “EH6” enstatite chondrites and implications for collisional heating of the EH and EL parent asteroids. *Geochim Cosmochim Acta* 75: 3757–3780
- SCHRADER DL, DAVIDSON J, MCCOY TJ, ZEGA TJ, RUSSEL SS, DOMANIK KJ, KING AJ (2021) The Fe/S ratio of pyrrhotite group sulfides in chondrites: An indicator of oxidation and implications for return samples from asteroids Ryugu and Bennu. *Geochim Cosmochim Acta* 303: 66–91
- SKÁLA R, DRÁBEK M (2005) Influence of titanium content on crystal structure of iron monosulfide (abstr.). 68th Annual Meeting of the Meteoritical Society, *Meteorit Planet Sci* 40: A143-A143
- SKÁLA R, CÍSAŘOVÁ I, DRÁBEK M (2006) Inversion twinning in troilite. *Amer Miner* 91: 917–921
- THOMPSON P, COX DE, HASTINGS JB (1987) Rietveld refinement of Debye-Scherrer synchrotron X-ray data from Al₂O₃. *J Appl Crystallogr* 20:79–83.
- TÖPEL-SCHADT J, MÜLLER WF (1982) Transmission electron microscopy on meteoritic troilite. *Phys Chem Miner* 8: 175–179
- VIEANE W, KULLERUD G (1971) The Ti-S and Fe-Ti-S systems. *Carnegie Inst Wash* 70: 297–299
- WATTERS TR, PRINZ M (1979) Aubrites: their origin and relationships to enstatite chondrites. *Proc Lunar Planet Sci Con* 10: 1073–1093
- WEISBERG MK, FOGEL RA, PRINZ M (1997) QUE 94204: An EH-chondritic melt rock (abstr. #1768) 28th Lunar and Planetary Science Conference: CD-ROM
- WEYRAUCH M, HORSTMANN M, BISCHOFF A (2018) Chemical variations of sulfides and metal in enstatite chondrites—Introduction of a new classification scheme. *Meteorit Planet Sci* 53: 394–415
- YAKOVLEVA OS, PEKOV IV, BRYZGALOV IA, MEN'SHIKOV YP (2010) Chalcogenide mineralization in the alumina-rich fenites of the Khibiny alkaline complex (Kola Peninsula, Russia). *New Data on Minerals* 5: 33–49
- ZHANG Y, BENOIT PH, SEARS DW (1995) The classification and complex thermal history of the enstatite chondrites. *J Geophys Res* 100: 9417–9438